catalysts

MDPI

Article

Enhancement of Photocatalytic Activities with Nanosized Polystyrene Spheres Patterned Titanium Dioxide Films for Water Purification

Hyeon Jin Seo [1], Ji Won Lee [2], Young Hoon Na [1] and Jin-Hyo Boo [1,2,*]

[1] Department of Chemistry, Sungkyunkwan University, Suwon 16419, Korea; qpzwoxeic@skku.edu (H.J.S.); yhna@hanmail.net (Y.H.N.)

[2] Institute of Basic Science, Sungkyunkwan University, Suwon 16419, Korea; ljw9917@naver.com

* Correspondence: jhboo@skku.edu; Tel.: +82-31-290-7072

Received: 22 July 2020; Accepted: 4 August 2020; Published: 5 August 2020

Abstract: For environmental applications, such as water and air purification utilizing photocatalysts, we synthesized patterned titanium dioxide (TiO_2) thin films using polystyrene (PS) spheres. This was primarily done to enhance the surface area and photocatalytic activities. TiO_2 thin films were deposited on silicon wafers attached to variously sized PS spheres via the spin coating method and were annealed at 600 °C. The processing step involved patterning and coating a TiO_2 sol–gel. The photocatalytic performance was analyzed using an UV–visible spectrophotometer. Within 20 min, a high catalytic efficiency (98% removal) with a 20-time faster decomposition rate of the malachite green (MG) solution than that of the nonpatterned TiO_2 was obtained from the patterned TiO_2 with 400 nm sized PS due to the large surface area. In addition, the phenol in the water removed as much as 50% within 2 h with the same photocatalyst, which was expected to be one of the strong candidates to be applied to the next generation of photocatalysts for water purification.

Keywords: titanium dioxide; photocatalyst; polystyrene sphere; patterned structure; dye and phenol removal

1. Introduction

The degradation of toxic materials from the biosphere is a multibillion dollar industry [1]. The most common methods rely on the use of high temperatures to accomplish the degradation, but such processes are expensive and must be carefully controlled, and the removal of effluent gases is challenging [2–5]. Textile, paper, dye, and pharmaceutical manufacturing facilities can contaminate water with residual dyes, which are mostly organic pollutants that are highly toxic and hazardous to humans and animals, and thus the removal of these organic contaminants prior to discharge into the environment is essential. Various insitu treatment methods based on bioremediation and electroreduction can be used, but each has inherent limitations [6]. Recently, a number of advanced, photocatalytic oxidation processes have been investigated, some of which appear to be promising alternatives, especially those that use natural sunlight as an energy input source [7–9]. In 1972, Fujishima and Honda demonstrated the potential of titanium dioxide (TiO_2) semiconductor materials to split water into hydrogen and oxygen in a photoelectrochemical cell [10]. Their work triggered the development of semiconductor photocatalysis for a wide range of environmental and energy applications [11]. TiO_2 is an example of a solid state semiconductor, characterized by two "bands"of closely spaced electronic energy levels known as the valence and conduction bands, which are respectively analogous to the lowest unoccupied molecular orbital (LUMO) and the highest occupied molecular orbital (HOMO). When electrons are promoted from the valence band to the conduction band, they become delocalized, and the substrate can conduct electricity (Scheme 1).

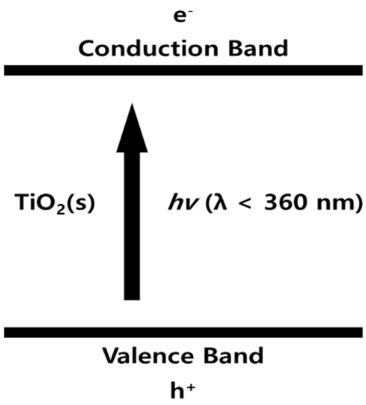

Scheme 1. Band energy structure of a typical solid state semiconductor, TiO_2.

Semiconductors have band gaps of intermediate energies between the conductor and insulator, and they can conduct if that band gap energy is supplied, thus elevating electrons from the valence into the conduction band. For anatase (a specific phase of TiO_2) and colloidal size regimes, this gap is roughly 320 $kJmol^{-1}$. Consequently, electronic excitation can be achieved by photons of light with λ being $\leq$ 360 nm [12]. Therefore, TiO_2 is a particularly important photocatalyst due to its oxidizing power, nontoxicity, and long-term photostability. Not only the electronic properties of a material but also its structure and morphology can have aconsiderable influence on its photocatalytic performance. Most photocatalytic tests were carried out both with TiO_2 nanoparticle suspensions (or 2D TiO_2 thin films), which are done under open circuit conditions, indicating that electron and hole transfer occur from the same particle, and in a photoelectrochemical two-electrode configuration where TiO_2 is generally used as a photoanode together with an inert or catalytic cathode such as Pt, C, etc. Over the past years, this is why nanotube geometries (particularly anodic TiO_2 nanotube layers) have gained a lot of interest due to various potential advantages. In recent years particularly, 1D structures such as nanowires and nanotubes have also received great attention for their use as a photoelectrode [13–16].

The most important factors that influence the photocatalysis of TiO_2 nanotubes are the crystallinity, length, and diameter of the tubes, together with compositional effects. In early reports, it was demonstrated that the nanotube layers can have a higher efficiency than comparable compacted nanoparticle layers [17]. As for particles and as expected from a point of zero charge of TiO_2 of approximately 6–7, for acidic pH typically a better adsorption of, for example, COO^- containing molecules (for example dyes) was observed, and typically at least slightly increased photocatalytic kinetics was observed [18]. As a powder particle, however, its use is somewhat inconvenient as it must be separated from the water in a slurry system after the photocatalytic reaction is complete. Accordingly, the development of a different method to apply TiO_2 coatings to various substrates is being pursued by researchers around the world [19–21].

Since the basic photocatalytic method investigated in our laboratory that used a colloidal suspension of titanium dioxide (TiO_2) has already been published [22], the main purpose of this study involves the synthesis of nanosized polystyrene (PS) patterned TiO_2 thin films to enhance both the surface area and the photocatalytic performance.

2. Results and Discussion

The synthesized PS colloidal monolayer patterned titanium dioxide films (with diameters of 400, 700, 1000, and 1300 nm, respectively) were characterized by field emission scanning electron microscopy (FE-SEM, Model JSM-7100 F) to evaluate their structures (Figure 1). The cross-sectional images (Figure 1e–h) show the monolayer patterned TiO_2 films on the PS spheres mask. The TiO_2 films with 1000 and 1300 nm sized patterns had well-ordered honeycomb-like structures (Figure 1c,d), but the TiO_2 films with 400 and 700 nm sized patterns had disordered structures (Figure 1a,b) and high surface charges. Therefore, smaller PS spheres had more difficulties aligning in the monolayer than the

larger PS spheres. However, as these samples had relatively higher surface are as compared with those of the bigger PS spheres, higher catalytic activity was expected.

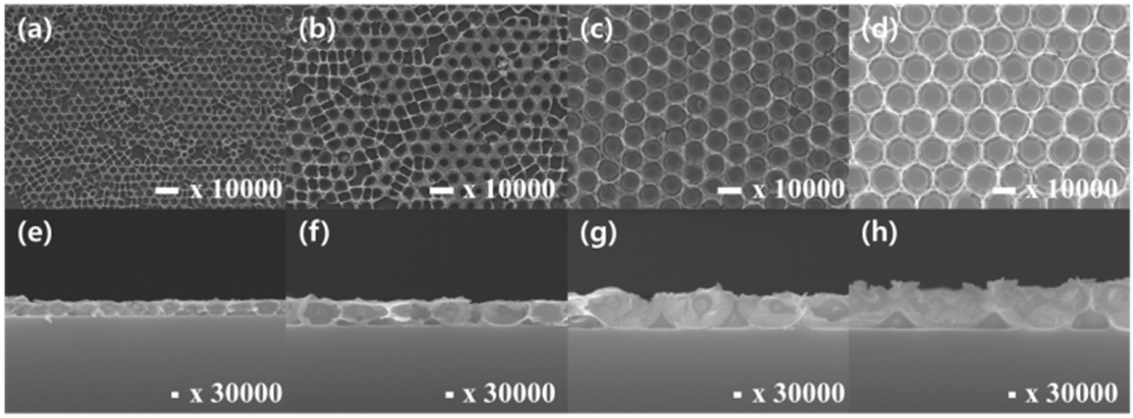

Figure 1. FE-SEM images of the top and cross-sectional views of the fabricated structures from the polystyrene(PS) patterned TiO_2 films with 400 nm (**a**,**e**), 700 nm (**b**,**f**), 1000 nm (**c**,**g**) and 1300 nm (**d**,**h**). Scale bars were 1000 nm for (**a**–**d**), and 3000 nm for (**e**–**h**).

The interesting thing is that the morphology of the PS-patterned TiO_2 films, based on the top-view SEM, is similar to that of anodic TiO_2 nanotubes [15]. Moreover, the AFM images (Figure 2) of the PS-patterned TiO_2 films are similar to that of TiO_2 nanotubes [16]. In this paper, therefore, the pros and cons of the PS-patterned TiO_2 films are described and then compared to those of anodic TiO_2 nanotubes. To mention briefly, the main advantage of this work is that it can control the height and distance of the pore size in PS-patterned TiO_2 films by varying the diameter of the PS sphere and adopting the oxygen plasma etching technique. However, compared to the anodic TiO_2 nanotubes, the PS-patterned TiO_2 films have limitations in the production of very thick TiO_2 films, which are inferior in terms of the specific surface area.

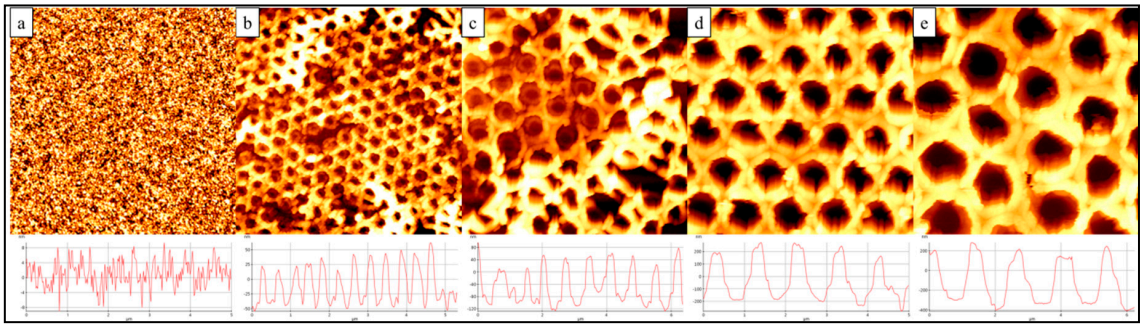

Figure 2. Atomicforce microscopy(AFM) images with line profiles of nonpatterned TiO_2 films (**a**) and PS-patterned TiO_2 films with diameters of 400 nm (**b**), 700 nm (**c**), 1000 nm (**d**) and 1300 nm (**e**).

Figure 2 depicts atomicforce microscopy (AFM) images, taken using an atomic force microscope (Park NX10-Atomic Force Microscope) of both nonpatterned PS-patterned TiO_2 thin films and the patterned TiO_2 using the PS spheres mask with diameters of 400, 700, 1000, and 1300 nm with the same silicon wafer. A surface morphology similar to that of FE-SEM was obtained. However, AFM images with line profiles show a different average depth of both the nonpatterned and PS-patterned TiO_2 thin films, as shown in the line profile range of 50, 100, 200, 400, and 500 nm, respectively (Figure 2). With these line profiles, the surface areas of both nonpatterned and PS-patterned TiO_2 thin films were obtained using an AFM-supported computer program. The calculated values for both PS-patterned (400, 700, 1000, and 1300 nm) and nonpatterned TiO_2 thin films were 67.8, 50.8, 43.4, 35.2, and 26.5 nm^2, respectively. Since it was very difficult to measure the Brunauer–Emmett–Teller (BET) surface area

of the 2D-thin films (especially for the nonpatterned and small-sized PS-patterned TiO_2 thin films) with very small pore volumes rather than those of 3D-powders, in this study, the surface area was measured using AFM instead of the BET method.

Figure 3 shows the crystallinity of the patterned TiO_2 film with a 400 nm size PS taken using X-ray diffractometer (XRD, D/Max Ultima III, Rigaku Corporation). The XRD patterns were found to have a main peak at $2\theta = 25.2°$, presumably due to the anatase (101) plane (JCPDS 21-1272), suggesting that all films mostly have a {101} facet, and there will be no influence of catalytic activity change on catalyst type. Peaks corresponding to the rutile and brookite phases were also not detected [23], and thus a high catalytic activity is expected.

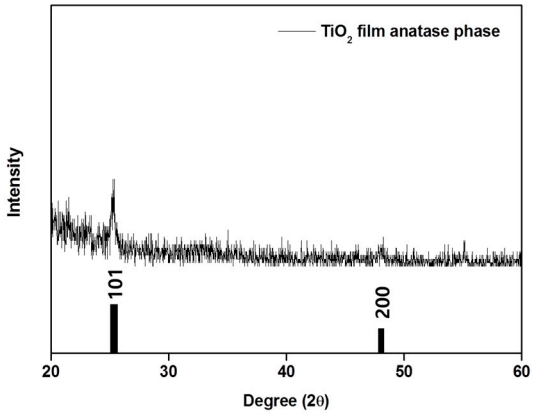

Figure 3. XRD pattern of the 400 nm size PS-patterned TiO_2 film.

X-ray photoelectron spectroscopy (XPS) measurements were made in order to observe the chemical state changes of PS-patterned TiO_2 thin films during the manufacturing process. In Figure 4, Ti $2p_{1/2}$ was observed at ~463 eV, and Ti $2p_{3/2}$ was observed at ~458 eV. For the PS-patterned TiO_2 thin films (400, 700, 1000, and 1300 nm), a chemical shift also occurred. However, it appears there was no distinct order and no binding energy difference for all samples [24]. Accordingly, there was no difference due to the defects of TiO_2 inducing by oxygen vacancy when making the films. Therefore, we concluded that all PS-patterned TiO_2 thin films were observed only for the Ti^{4+} chemical state. In particular, only small changes in relative intensity (400 > 700 > 1000 > 1300 nm) of the TiO_2 films with PS patterns were observed. This means that the intensity of XPS spectra changes very little; therefore, it is suggested that as the PS size decreases, the amount of the TiO_2 increases and the intensity of the XPS spectrum increases when decreasing the PS sizes. In other word, the same sequence such as the relative intensity (400 > 700 > 1000 > 1300 nm) of PS-patterned TiO_2 thin films was obtained because of the same mean free path of the electron in the TiO_2 film layers under the same energy ranges of X-ray photoelectrons, even though the samples have different thickness. These results would be closely related with the values of the surface area.

For testing of photocatalytic activity, amalachite green (MG: $C_{23}H_{25}ClN_2$) solution was prepared by dissolving 0.001 g of MG in 1000 mL of distilled water. The concentration of this solution was 2.74×10^{-6} M. The prepared PS-patterned TiO_2 films on 20×20 mm^2 sized silicon wafers were placed in a two-inch plastic dish, which was filled with 10 mL of MG solution. The plastic dish was placed in a black box and irradiated using ultraviolet (UV) light with a wavelength of 254 nm. Using an UV–visible spectrometer, the absorption spectrum of the MG solution was measured for 120 min, and the results are plotted in Figure 5. The inset of Figure 5 depicts the initial decomposition behavior (enlarged plot of the Figure 5 from 0 to 25 min) of the MG solution with 400–1300 nm PS-patterned TiO_2 films. As shown in the inset of Figure 5, within 20 min, all the PS-patterned photocatalysts tested in this study decomposed at least 95% or more of the MG molecules present. Complete decomposition of the MG solution occurred after 120 min. However, use of the nonpatterned TiO_2 films resulted in

only 63% degradation of the MG solution after 120 min. Of the catalysts tested, the highest efficiency (98% removal) resulted from use of the patterned TiO_2 with 400 nm size PS, perhaps due to the large surface area. This result clearly shows that PS patterning can increase the photocatalytic efficiency as much as 20 times higher than that of nonpatterned TiO_2 film in the initial 20 min. The introduction of porous channels into macroporous TiO_2 increased the photocatalytic activity due to the minimization of intradiffusion resistance and the enhancement of photoabsorption efficiency [25]. In the 3D materials, the macrochannels can serve as effective paths for light and reactant transportation. This allows the UV light to penetrate more deeply inside the porous TiO_2 films, resulting in the enhancement of degradation efficiency and rate of MG by TiO_2 photocatalysts fabricated with PS patterning with a different diameter [26].

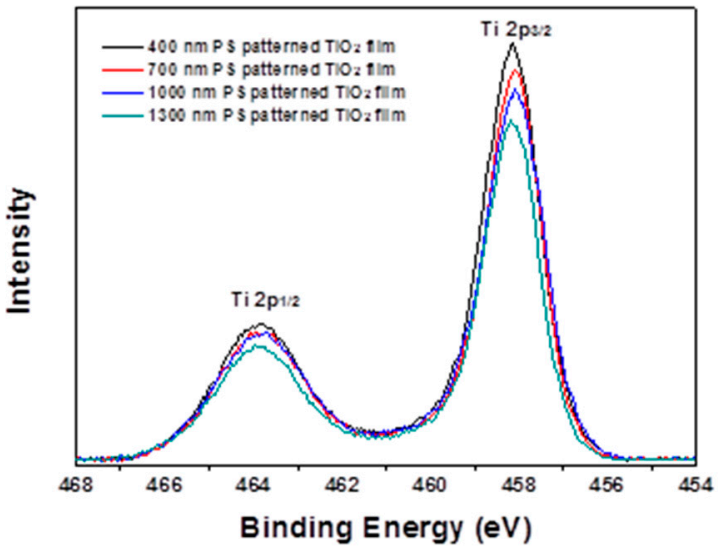

Figure 4. High resolution Ti 2p X-ray photoelectron (XP) spectra of the TiO_2 photocatalysts synthesized with 400 nm, 700 nm, 1000 nm, and 1300 nm patterned TiO_2 films.

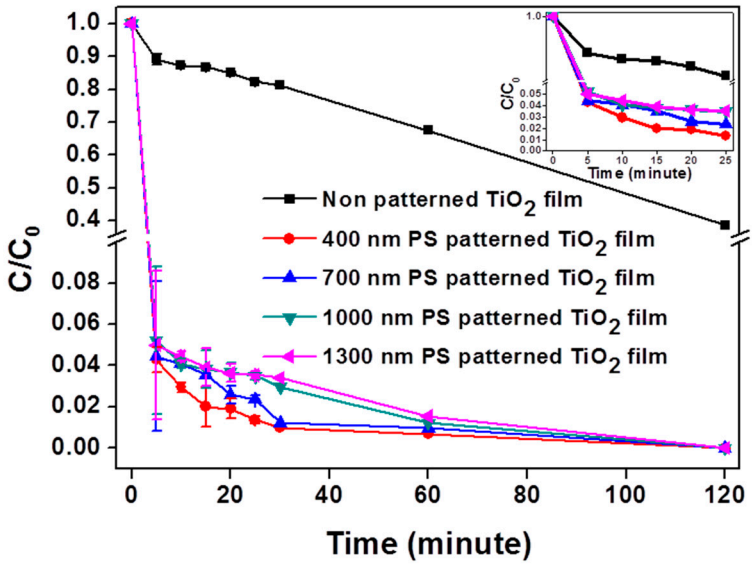

Figure 5. Photocatalytic degradation of malachite green (MG) with the nonpatterned TiO_2 film and PS-patterned TiO_2 films. Inset shows photocatalytic degradation of MG for initial 25 min.

As we mentioned before, there are many factors that influence the photocatalysis of both TiO_2 nanotubes and particles (in this case the PS-patterned TiO_2 films). Among them, we will consider the length, diameter, together with surface area. For example, a report of either a maximum in the photocatalytic activity for tube layer thicknesses around 3–7 μm [27,28] or the absence of an influence of the tube length [29] was announced. In addition, there is a discrepancy for the influence of tube diameter. For example, one report announced no significant influence [30,31], but the other report showed maximum photocatalytic efficiency at around −100 nm [28,32], or other trends [33]. These discrepancies can be attributed to the fact that it is very difficult to vary tube length independently from tube diameter. Besides TiO_2 nanotubes, there are also reports about other forms of self-organized structures such as self-organized mesoporous TiO_2 [34]. These structures, named as "titaniamesosponge"(TMS) or "nanochannelar"structures, can contain significant crystallinity (anatase and anatase/rutile) and when annealed can show an enhanced photocatalytic activity as compared to P25 layers, depending on layer thickness and annealing conditions (i.e., different surface area) [35]. Since our PS-patterned TiO_2 films have a similarity to TiO_2 nanotubes, both parameters (such as diameter, thickness layers, morphology/crystallinity, and annealing at 600 °C) will affect the photocatalytic activities, resulting in a 20-time faster decomposition rate of MG dye solution with 400 nm PS-patterned TiO_2 film compared with that of nonpatterned TiO_2. However, a more detailed kinetic study including detection of key radicals such as O(1D) and OH· radicals is highly desirable to clarify our amazing result. It is well known that the average lifetime of OH radical (τOH) in an ambient atmospheric condition is around 0.01–1 s [36], which is affected by the concentration of reactive gas components such as ozone, VOCs, and NOx.

From an application viewpoint, the most important reactions are the transfer of valence band electronsto H_2O, H^+, or O_2 and the transfer of holes to H_2O, OH^-, or organic species. If we consider an aqueous environment, then the transfer of conduction band electrons may lead to the production of H_2. For the valence band holes, except for a reaction with OH^- or H_2O to form O_2, OH· radical formation may also occur and is often the desired reaction for pollution degradation. In this case, formed OH· radicals are able to virtually decompose all organics to CO_2 + H_2O. Nevertheless, if the H_2O concentration is comparably small, valence band holes may also be transferred directly to the organics and lead to their decomposition. Theoretically, therefore, maximum efficiency for the photocatalytic reaction is when all charge carriers react with the species from the surroundings rather than recombine.

To understand this in detail, the efficiency of MG dye decomposition and the surface area of the PS-patterned TiO_2 thin films were compared after irradiating 254 nm UV light into the PS-patterned thin films for 120 min (Figure 6). The surface area was calculated by AFM, as shown in the part of Figure 2, to allow for an accurate comparison of the patterns according to the PS size of 400, 700, 1000, and 1300 nm. Based on Figure 5, the maximum degradation efficiencies, such as 97.8%, 96.6%, 96.0%, 95.6%, and 63.0% (not shown in Figure 6), were obtained from both PS-patterned (400, 700, 1000, and 1300 nm) and nonpatterned TiO_2 thin films, respectively. As a result of the surface area calculation, from Figure 6, we realized that the degradation efficiency improved in proportion to the surface area. This means that there will be a close relationship between the photocatalytic efficiency and the surface area, and a detailed mechanism supporting this relationship should highly be desirable for clarifying results [37,38].

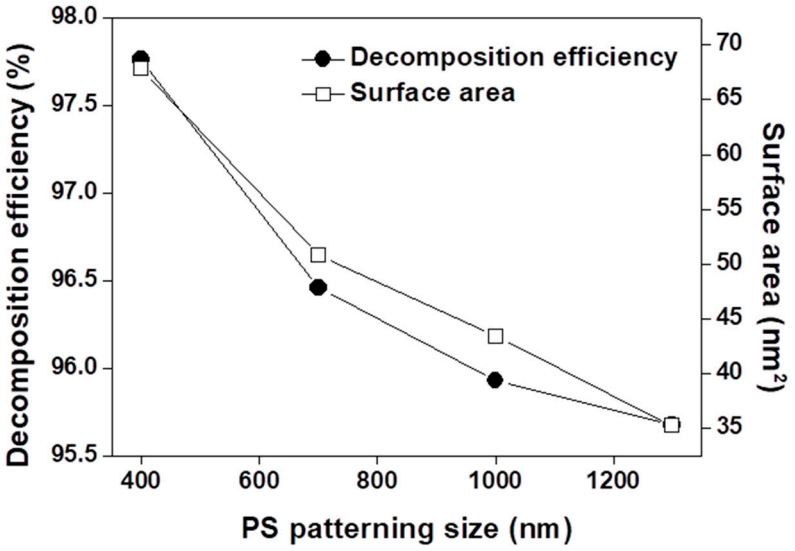

Figure 6. The initial photodegradation efficiency of PS-patterned films irradiated with a UV lamp for 25 min and the variations of surface area among the PS-patterned films.

Based on our experimental data, especially shown in the inset of Figure 5, the reaction constants of both nonpatterned TiO_2 and PS-patterned TiO_2 were calculated using the following equation by assuming the first-order kinetics.

$$\begin{gathered} \text{The reaction rate} = -\frac{d[\mathrm{C}]}{dt} = k[\mathrm{C}] \\ \frac{1}{k}\int_{[\mathrm{C}]_0}^{[\mathrm{C}]_t} \frac{1}{[\mathrm{C}]} \times d[\mathrm{C}] = -\int_0^t dt \\ \frac{1}{k} \times (\ln[\mathrm{C}] - \ln[\mathrm{C}]_0) = -t \end{gathered} \quad (1)$$

$$\ln(\mathrm{C}/\mathrm{C}_0) = -kt \quad (2)$$

$$\mathrm{C} = \mathrm{C}_0 \exp(-kt) \quad (3)$$

where C_0 and C are the initial concentration and the concentration of MG solution, respectively; t is the photoreaction time; and k is the reaction constant. Equation (3) has the form of an exponential decay (similar to theinset of Figure 5). A common feature of all first-order reactions, therefore, is that the concentration of the reactant (i.e., the MG photodegradation in this study) decays exponentially with time. However, there are different exponential decay curves depending on k values. The greater the rate constant, the more rapid is the decay curve. Based on the Equation (2), we can get the rate constants (k_1/min) from each decay curve. Figure 7a shows a plot of $\ln(C/C_0)$ versus the photocatalytic reaction time (t) for both the nonpatterned TiO_2 film and the 400 nm PS-patterned TiO_2 film irradiated with 254 nm UV light for 25 min under the same experimental condition. From the slopes of each plot, the rate constants (k_{obs}/min) of 0.0064 and 0.140 were obtained. From the similar experiments on the PS-patterned (700, 1000, and 1300 nm) TiO_2 films, the rate constants (k_{obs}/min) with 0.117, 0.102, and 0.101 were also obtained, respectively (not shown in Figure 7a). Figure 7b shows variation of the rate constant with the PS diameter. In increasing the PS diameter from 400 to 1300 nm, there was a decreasing tendency of rate constant from 0.14 to 0.10. The perfect linearity indicates the first-order kinetics with the first-order rate constant (k_1/min), but the experimentally obtained data in this work have large deviations, suggesting a pseudo first-order kinetics (not perfect first-order reaction) with pseudo first-order rate constants (k_{obs}/min). Therefore, Figure 7 provides us small hints regarding the effects of the initial MG concentration on the removal efficiency. First, the TiO_2 thin film patterned with 400 nm PS beads was observed to decompose the MG dye the most rapidly (20 times faster than nonpatterned TiO_2 thin film). Second, the photocatalytic degradation of MG in both the 400 nm

size PS-patterned and nonpatterned TiO_2 thin films exhibits pseudo first-order kinetics with different rate constants (k_{obs}) [39]. This means that the kinetics of photocatalytic degradation of MG in both nonpatterned and PS-patterned TiO_2 thin films were the same, but there were large differences in value (maximum 22 times) of the rate constants between nonpatterned and PS-patterned TiO_2 thin films. It is very important to note that a rate law is established experimentally and cannot in general be inferred from the chemical equation for the reaction. Moreover, the reaction order can only be determined experimentally. Since we did not measure either the half-life (which is independent of reactant concentration for the first-order kinetics) or the time constant (i.e., lifetime; the longer the time constant of the first-order reaction, the slower the decay and the longer the reaction survives) by a laser spectroscopic technique, further experimentation is highly desirable for determining the exact reaction kinetics.

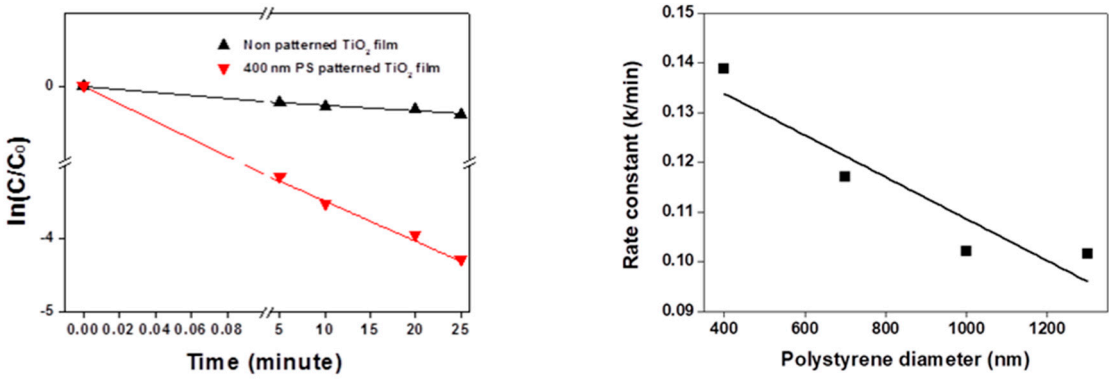

(**a**) (**b**)

Figure 7. (**a**) Effect of initial MG concentration on the removal efficiency: the plot of $\ln(C/C_0)$ versus irradiation time for the nonpatterned TiO_2 film and the 400 nm PS-patterned TiO_2 film for 25 min. (**b**) Variation of rate constant with PS diameter. The perfect linearity indicates the first-order kinetics with the first-order rate constant (k_1/min), but the experimental data have deviations, suggesting a pseudofirst-order rate constants (k_{obs}/min).

For environmental application such as water purification [37], a phenol degradation experiment was also performed using the best catalyst to determine the ability of the patterned TiO_2 films to purify water. Figure 8 depicts the photodegradation of phenol in the presence of 400 nm PS-patterned TiO_2 films. The photocatalytic performance measurements were carried out by exposing the 400 nm PS-patterned TiO_2 film to UV light with a wavelength of 254 nm while soaking it in a 200 ppm solution of phenol solution for 120 min. Phenol exposed to UV light for 120 min was decomposed until a concentration of 100 ppm was reached (50% removal within 2 h), suggesting that the proposed PS-patterned TiO_2 thin film will be one of the possible strong candidates for new types of photocatalysts for both dye decomposition and water purification. This suggests that it is especially important for future applications in environmental purification processes to develop PS-patterned TiO_2 films on non flat supports such as 3D meshes/grids, spheres, or others with good adhesion [40].

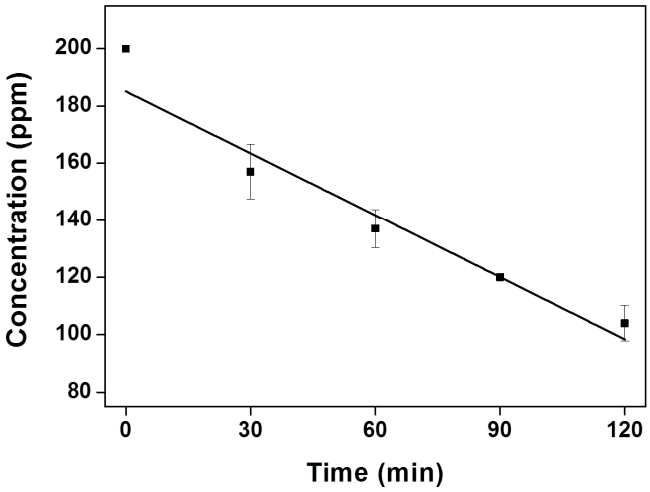

Figure 8. Photocatalytic degradation of phenol in the presence of the 400 nm PS-patterned TiO_2 film.

3. Materials and Methods

3.1. Preparation of Polystyrene (PS) Spheres

The size of the polystyrene (PS) spheres affects the reaction time during the dispersion and polymerization of styrene. With increasing reaction time, the size of the PS spheres increased proportionally (400, 700, 1000, and 1300 nm). An ordered PS sphere monolayer was generated using the conventional air–water interface mediated method. This indicated that blowing led to an improvement in the crystal domain size by facilitating recrystallization during the self-assembly process. Before growing, the apertures of the PS monolayer were modified by thermal treatment in a tube furnace, which ensures uniformity throughout the sample and allows for good control over the aperture size by an adjustment of the adhesion time. Adhesion was achieved by using a hot plate at 120 °C. Field emission scanning electron microscopy (FE-SEM, JEOL Corp., Model JSM-7100 F, Tokyo, Japan) images (Figure 1) of the synthesized PS spheres show highly uniform diameters.

3.2. Preparation of the TiO_2 Sol–Gel

The TiO_2 sol–gel catalysts (pH= 2.2 and 5.7 wt%) were prepared by mixing titanium hydroxide oxide ($Ti(OH)_2O$) with hydrochloric acid (HCl) at a molar ratio of 1:3 in ethanol. The solution was stirred at 80 °C for 2 h, and concentrated in vacuum to give a white slurry. The slurry was then kept for 1 day at 80 °C in an electric oven, after which it turned into a yellow powder, which was annealed in the furnace at 600 °C for 17 min.

3.3. Synthesis of Nonpatterned and PS-Patterned TiO_2 Thin Films

Silicon (100) wafers (20 x 20 mm^2) were cleaned by sonication with acetone (10 min), ethyl alcohol (10 min), and distilled water (10 min), followed by drying with N_2 gas. The cleaned silicon wafers were treated with oxygen plasma to enhance the adhesion of variously sized PS spheres at 100 Watts, 100 sccm, and 5 min. PS beads of various sizes were arranged on the silicon wafers to increase the surface area, using 400, 700, 1000, and 1300 nm for a monolayer coating as well as the PS spheres. After this, 200 µL of TiO_2 sol–gel was dropped onto the PS-patterned silicon wafers and allowed to sit for 1 min. Afterward, the PS substrates were coated using the spin coating method (3000 rpm, 30 s) and annealed in a furnace at 600 °C for 6 h to provide PS-patterned TiO_2 films. Nonpatterned TiO_2 films were produced in the same way as PS-patterned TiO_2 films but without a PS monolayer coating. The detailed deposition process of the nonpatterned TiO_2 films was already published elsewhere [16].

3.4. The Methods of Photocatalytic Activity Measurements

Catalytic degradations of both a malachite green (MG) solution and phenol in water by various PS-patterned TiO_2 films were undertaken to evaluate the catalytic efficiency of the films, which was monitored using UV–visible absorption spectroscopy (UV-3600 Plus UV-VIS-NIR Spectrophotometer: SHIMADZU, Kyoto, Japan). For testing of photocatalytic activity, a MG($C_{23}H_{25}ClN_2$) solution with a concentration of 2.74×10^{-6} M was prepared. The prepared PS-patterned TiO_2 films on 20×20 mm^2 sized silicon wafers were placed in a two-inch plastic dish, which was filled with 10 mL of MG solution. The plastic dish was placed in a black box and irradiated using ultraviolet (UV) light with a wavelength of 254 nm and a power of 10 W (Spectroline, NY, USA). Using an UV–visible spectrometer, the absorption spectrum of the MG solution was measured in the wavelength range between 400 and 800 nm for 120 min. The phenol degradation measurements were also carried out by exposing the 400 nm PS-patterned TiO_2 film to UV light with a wavelength of 254 nm while soaking it in a 200 ppm solution of phenol solution for 120 min (Sigma-Aldrich, St. Louis, USA).

4. Conclusions

In this study the polystyrene (PS)-patterned TiO_2 thin films were synthesized to enhance both the surface area and the photocatalytic performance. In the photocatalytic efficiency test, all patterned TiO_2 thin films decomposed MG dye almost 100% while the nonpatterned TiO_2 thin films decomposed MG dye by about 63% in 120 min, and a 20-time higher photocatalytic decomposition rate of MG dye was obtained within 20 min with 400 nm PS-patterned TiO_2 thin film compared with that of nonpatterned TiO_2 film. For water purification, a phenol degradation experiment was also performed using the same photocatalyst, resulting in the removal of phenol in the water as much as 50% within 2 h.

However, the kinetics of MG dye decomposition shows the same mechanism (pseudo first-order kinetics). All the TiO_2 films tested were capable of decomposing harmful material such as phenol into the patterned film, but the highest performing thin film was for the 400 nm PS sphere patterned thin film. Since the process used to layer the TiO_2 onto the PS spheres was cheaper and easier than previous methods, and it was also amenable to large area substrates, future studies to further develop this technology are highly expected. Because this is especially important for future applications in environmental purification processes, we have to develop a technique on preparing a catalyst onto both flat and non flat supports with good adhesion.

Author Contributions: Conceptualization, H.J.S and J.-H.B.; methodology, Y.H.N.; software, J.W.L; validation, H.J.S., J.W.L. and J.-H.B.; formal analysis, H.J.S.; investigation, Y.H.N.; resources, J.-H.B.; data curation, H.J.S.; writing—original draft preparation, H.J.S.; writing—review and editing, J.-H.B.; visualization, J.W.L.; supervision, J.-H.B.; project administration, J.-H.B.; funding acquisition, J.-H.B. All authors have read and agreed to the published version of the manuscript.

Funding: This work was supported by the National Research Foundation of Korea (NRF) grant funded by the Korea government (MSIT) (2020R1A2C1011764).

Conflicts of Interest: The authors declare no conflict of interest.

References

1. Thakur, M.; Sharma, G.; Ahamad, T.; Ghfar, A.A.; Pathania, D.; Naushad, M. Efficient photocatalytic degradation of toxic dyes from aqueous environment using gelatin-Zr(IV) phosphate nanocomposite and its antimicrobial activity. *Colloids Surf. B* **2017**, *157*, 456–463. [CrossRef] [PubMed]
2. Santhosh, C.; Malathi, A.; Daneshvar, E.; Kollu, P.; Bhatnagar, A. Photocatalytic degradation of toxic aquatic pollutants by novel magnetic 3D-TiO_2@HPGA nanocomposite. *Sci. Rep.* **2018**, *8*, 15531–15545. [CrossRef] [PubMed]
3. Shanker, U.; Jassal, V.; Rani, M. Green synthesis of iron hexacyanoferrate nanoparticles: Potential candidate for the degradation of toxic PAHs. *J. Environ. Chem. Eng.* **2017**, *5*, 4108–4120. [CrossRef]

4. Sajid, M.M.; Amin, N.; Shad, N.A.; Khan, S.B.; Javed, Y.; Zhang, Z. Hydrothermal fabrication of monoclinic bismuth vanadate (m-$BiVO_4$) nanoparticles for photocatalytic degradation of toxic organic dyes. *Mater. Sci. Eng. B* **2019**, *242*, 83–89. [CrossRef]
5. Wang, C.; Zuo, Y.; Yang, C.-L. Selective catalytic reduction of NO by NH_3 in flue gases over a Cu-V/Al_2O_3 catalyst at low temperature. *Environ. Eng. Sci.* **2009**, *26*, 1429–1434. [CrossRef]
6. Wu, Y.; Jing, X.; Gao, C.; Huang, Q.; Cai, P. Recent advances in microbial electrochemical system for soil bioremediation. *Chemosphere* **2018**, *211*, 156–163. [CrossRef] [PubMed]
7. Mamaghani, A.H.; Haghighat, F.; Lee, C.-S. Role of titanium dioxide (TiO_2) structural design/morphology in photocatalytic air purification. *Appl. Catal. B Environ.* **2020**, *269*, 118735–118752. [CrossRef]
8. Boyjoo, Y.; Sun, H.; Liu, J.; Pareek, V.K.; Wang, S. A review on photocatalysis for air treatment: From catalyst development to reactor design. *Chem. Eng. J.* **2017**, *310*, 537–559. [CrossRef]
9. Mamaghani, A.H.; Haghighat, F.; Lee, C.-S. Photocatalytic oxidation technology for indoor environment air purification: The state-of-the-art. *Appl. Catal. B Environ.* **2017**, *203*, 247–269. [CrossRef]
10. Fujishima, A.; Honda, K. Electrochemical photolysis of water at a semiconductor electrode. *Nature* **1972**, *238*, 37–38. [CrossRef]
11. Nolan, N.T.; Seery, M.K.; Pillai, S.C. Spectroscopic investigation of the anatase-to-rutile transformation of sol-gel-synthesized TiO_2 photocatalyst. *J. Phys. Chem. C* **2009**, *113*, 16151–16157. [CrossRef]
12. Zuo, Y.; Zhang, K.; Zhou, S. Determination of estrogenic steroids and microbial and photochemical degradation of 17α-ethinylestradiol(EE2) in lake surface water, a case study. *Environ. Sci. Process. Impacts* **2013**, *15*, 1529–1535. [CrossRef]
13. Li, S.; Liu, C.; Chen, P.; Lv, W.; Liu, G. In-situ stabilizing surface oxygen vacancies of TiO_2 nanowire array photoelectrode by N-doped carbon dots for enhanced photoelectrocatalytic activities under visible light. *J. Catal.* **2020**, *382*, 212–227. [CrossRef]
14. Cheng, X.; Cheng, Q.; Deng, X.; Wang, P.; Liu, H. A facile and novel strategy to synthesize reduced TiO_2 nanotubes photoelectrode for photoelectrocatalytic degradation of diclofenac. *Chemosphere* **2016**, *144*, 888–894. [CrossRef] [PubMed]
15. Lee, K.; Mazare, A.; Schmuki, P. One-dimensional titanium dioxide nanomaterials: Nanotubes. *Chem. Rev.* **2014**, *114*, 9385–9454. [CrossRef]
16. Sopha, H.; Tesar, K.; Knotek, P.; Jager, A.; Hromadko, L.; Macak, J.M. TiO_2 nanotubes grown on Ti substrates with different microstructure. *J. Mater. Res. Bull.* **2018**, *103*, 197–204. [CrossRef]
17. Macak, J.M.; Zlamal, M.; Krysa, J.; Schmuki, P. Self-organized TiO_2 nanotube layers as highly efficient photocatalysts. *Small* **2007**, *3*, 300–304. [CrossRef] [PubMed]
18. Sohn, Y.S.; Smith, Y.R.; Misra, M.; Subramanian, V.R. Electrochemically assisted photocatalytic degradation of methyl orange using anodized titanium dioxide nanotubes. *Appl. Catal. B Environ.* **2008**, *84*, 372–378. [CrossRef]
19. Cheng, Z.; Cheng, K.; Weng, W. SiO_2/TiO_2 nanocomposite films on polystyrene for light-induced cell detachment application. *ACS Appl. Mater. Interfaces* **2017**, *9*, 2130–2137. [CrossRef]
20. Riaz, S.; Ashraf, M.; Hussain, T.; Hussain, M.T.; Younus, A. Fabrication of robust multifaceted textiles by application of functionalized TiO_2 nanoparticles. *Colloids Surf. A* **2019**, *581*, 123799–123811. [CrossRef]
21. Ivanova, I.; Schneider, J.; Gutzmann, H.; Kliemann, J.-O.; Gartner, F.; Klassen, T.; Bahnemann, D.; Mendive, C.B. Photocatalytic degradation of oxalic and dichloroacetic acid on TiO_2 coated metal substrates. *Catal. Today* **2013**, *209*, 84–90. [CrossRef]
22. Nam, S.H.; Kim, T.K.; Boo, J.-H. Physical property and photo-catalytic activity of sulfur doped TiO_2 catalysts responding to visible light. *Catal. Today* **2012**, *185*, 259–262. [CrossRef]
23. Zhang, J.; Zhou, P.; Liu, J.; Yu, J. New understanding of the difference of photocatalytic activity among anatase, rutile and brookite TiO_2. *Phys. Chem. Chem. Phys.* **2014**, *16*, 20382–20386. [CrossRef] [PubMed]
24. Khan, M.M.; Ansari, S.A.; Pradhan, D.; Ansari, M.O.; Han, D.H.; Lee, J.T.; Cho, M.H. Band gap engineered TiO_2 nanoparticles for visible light induced photoelectrochemical and photocatalytic studies. *J. Mater. Chem. A* **2014**, *2*, 637–644. [CrossRef]
25. Wang, X.; Yu, J.C.; Hou, Y.; Fu, X. Photocatalytic activity of a hierarchically macro/mesoporous titania. *Langmuir* **2005**, *21*, 2552–2559. [CrossRef]
26. Liang, Y.; Guo, N.; Li, L.; Li, R.; Ji, G.; Gan, S. Fabrication of porous 3D flower-like Ag/ZnO heterostructure composite with enhanced photocatalytic performance. *Appl. Surf. Sci.* **2015**, *332*, 32–39. [CrossRef]

27. Roy, P.; Dey, T.; Lee, K.; Kim, D.; Fabry, B.; Schmuki, P. Size-selective separation of macromolecules by nanochannel titania membrane with self-cleaning (declogging) ability. *J. Am. Chem. Soc.* **2010**, *132*, 7893–7895. [CrossRef]
28. Liu, Z.; Zhang, X.; Nishimoto, S.; Murakami, T.; Fujishima, A. Efficient photocatalytic degradation of gaseous acetaldehyde by highly ordered TiO_2 nanotube arrays. *Environ. Sci. Technol.* **2008**, *42*, 8547–8551. [CrossRef]
29. Liang, H.-C.; Li, X.-Z. Effects of structure of anodic TiO_2 nanotube arrays on photocatalytic activity for the degradation of 2,3-dichlorophenol in aqueous solution. *J. Hazard. Mater.* **2009**, *162*, 1415–1422. [CrossRef]
30. Paramasivam, I.; Jha, H.; Liu, N.; Schmuki, P. A review of photocatalysis using self-organized TiO_2 nanotubes and other ordered oxide nanostructures. *Small* **2012**, *8*, 3073–3103. [CrossRef]
31. Zhuang, H.-F.; Lin, C.-J.; Lai, Y.-K.; Sun, L.; Li, J. Some critical structure factors of titanium oxide nanotube array in its photocatalytic activity. *Environ. Sci. Technol.* **2007**, *41*, 4735–4740. [CrossRef] [PubMed]
32. Smith, Y.R.; Kar, A.; Subramanian, V.R. Investigation of physicochemical parameters that influence photocatalytic degradation of methyl orange over TiO_2 nanotubes. *Ind. Eng. Chem. Res.* **2009**, *48*, 10268–10276. [CrossRef]
33. Ku, Y.; Fan, Z.-R.; Chou, Y.-C.; Wang, W.-Y. Effects of TiO_2 nanotube array dimension and annealing temperature on the acid red 4 degradation in aqueous solution by photocatalytic process. *Water Sci. Technol.* **2010**, *61*, 2943–2949. [CrossRef] [PubMed]
34. Kim, D.; Lee, K.; Roy, P.; Birajdar, B.I.; Spiecker, E.; Schmuki, P. Formation of a non-thickness-limited titanium dioxide mesosponge and its use in dye-sensitized solar cells. *Angew. Chem.* **2009**, *121*, 9490–9493. [CrossRef]
35. Lee, K.; Kim, D.; Roy, P.; Paramasivam, I.; Birajdar, B.I.; Spiecker, E.; Schmuki, P. Anodic formation of thick anatase TiO_2 mesosponge layers for high-efficiency photocatalysis. *J. Am. Chem. Soc.* **2010**, *132*, 1478–1479. [CrossRef]
36. Gligorovski, S.; Strekowski, R.; Barbati, S.; Vione, D. Environmental implications of hydroxyl radicals. *Chem. Rev.* **2015**, *115*, 13051–13092. [CrossRef]
37. Ling, H.; Kim, K.D.; Liu, Z.; Shi, J.; Zhu, X.; Huang, J. Photocatalytic degradation of phenol in water on as-prepared and surface modified TiO_2 nanoparticles. *Catal. Today* **2015**, *258*, 96–102. [CrossRef]
38. Jin, Z.; Zhang, Q.; Yuan, S.; Ohno, T. Synthesis high specific surface area nanotube g-C_3N_4 with two-step condensation treatment of melamine to enhance photocatalysis properties. *RSC Adv.* **2015**, *5*, 4026–4029. [CrossRef]
39. Doong, R.-A.; Chang, S.-M.; Hung, Y.-C.; Kao, I.-L. Preparation of highly ordered titanium dioxide porous films: Characterization and photocatalytic activity. *Sep. Purif. Technol.* **2007**, *58*, 192–199. [CrossRef]
40. Motola, M.; Dworniczek, E.; Satrapinskyy, L.; Chodaczek, G.; Grzesiak, J.; Gregor, M.; Plecenik, T.; Nowicka, J.; Plesch, G. UV light-induced photocatalytic, antimicrobial, and antibiofilm performance of anodic TiO_2 nanotube layers prepared on titanium mesh and Ti sputtered on silicon. *Chem. Pap.* **2019**, *73*, 1163–1172. [CrossRef]